Dominant Kitaev interactions on the fcc lattice in iridate double perovskites La_2BIrO_6 (B = Mg, Zn)

A. A. Aczel,[1,*] A. M. Cook,[2] T. J. Williams,[1] S. Calder,[1] A. D. Christianson,[1]
G.-X. Cao,[3] D. Mandrus,[3,4] Y. B. Kim,[2,5] and A. Paramekanti[2,5,†]

[1]*Quantum Condensed Matter Division, Oak Ridge National Laboratory, Oak Ridge, TN 37831, USA*
[2]*Department of Physics, University of Toronto, Toronto, Ontario, Canada M5S 1A7*
[3]*Materials Science and Technology Division, Oak Ridge National Laboratory, Oak Ridge, TN 37831, USA*
[4]*Department of Materials Science and Engineering, University of Tennessee, Knoxville, TN 37996, USA*
[5]*Canadian Institute for Advanced Research, Toronto, Ontario, M5G 1Z8, Canada*

(Dated: September 1, 2018)

We have performed inelastic neutron scattering experiments to investigate the magnetic excitations in the quasi-face-centered-cubic (fcc) iridate double perovskites La_2ZnIrO_6 and La_2MgIrO_6, which are characterized by A-type antiferromagnetic ground states. The neutron scattering data, which reveal gapped spin wave excitations with a very weak dispersion, are shown to be well-described by theoretical calculations on a model Hamiltonian with dominant Kitaev interactions. Our surprising finding shows that in contrast to honeycomb materials, where the Kitaev interaction manifests itself via complex magnetic order, even *conventional* magnetic orders in certain geometrically frustrated systems might owe their existence to unconventional Kitaev exchange.

PACS numbers: 75.30.Ds, 75.30.Et, 75.47.Lx

Transition metal (TM) compounds containing heavy atoms separated by ligands, such as TM oxides and TM halides, are often governed by spin-orbit coupling (SOC) and electronic correlations of comparable strength. The relativistic entanglement of correlated orbital and spin degrees of freedom in such materials can drive exotic quantum states of matter, such as $j_{\rm eff}=1/2$ Mott insulators [1], topological superconductors [2], topological insulators [3–5], Weyl semimetals [6], and quantum spin liquids [7]. For $j_{\rm eff} = 1/2$ magnetic atoms on the two-dimensional (2D) honeycomb lattice, featuring edge-sharing metal-ligand octahedra, this entanglement can lead to a complete cancellation of the conventional Heisenberg magnetic superexchange via TM-ligand-TM pathways. Consequently, the effective magnetic interaction can realize the highly anisotropic 'Kitaev model' [7], a remarkable Hamiltonian which is exactly solvable, with a quantum spin liquid ground state and emergent Majorana fermion excitations [8]. In materials such as α-Li_2IrO_3 [9], Na_2IrO_3 [10], and α-$RuCl_3$ [11], additional interactions, e.g., Heisenberg, off-diagonal exchange [12], or further neighbor interactions, are non-negligible, and lead to ordered ground states [13, 14]. However, Raman [15] and inelastic neutron scattering [16] measurements, in particular, have provided evidence of strong Kitaev interactions in α-$RuCl_3$, suggesting close proximity to a quantum spin liquid with deconfined spinon excitations. Recent experiments on the 3D honeycomb polymorphs β/γ-Li_2IrO_3 [17, 18] have uncovered complex spiral orders [19, 20], again ascribed to significant Kitaev exchange.

The common motifs in these previously studied materials are the three-fold coordination of the TM sites, the bipartite lattice structure, and the emergence of competing Heisenberg interactions between nearby TM atoms due to extended 4d/5d orbitals. Thus, it would be interesting to explore new physics which arises from breaking these motifs. Do materials with distinct local coordination exhibit new types of magnetic Hamiltonians? Does SOC on non-bipartite lattices enhance or inhibit geometric frustration? In materials with 5d atoms spaced further apart, can the resulting suppression of direct Heisenberg exchange lead to dominant Kitaev interactions?

Motivated by these questions, we study two recently synthesized iridate Mott insulators, the double perovskite (DP) materials La_2BIrO_6 (B=Mg, Zn) [21–24], with Ir^{4+} ions on the quasi-face-centered cubic (quasi-fcc) lattice. In these materials, the local octahedral environment of the Ir^{4+} ions is very close to the cubic limit, and the larger Ir-Ir distance compared with ABO_3 perovskites leads to a strong Mott insulator; these features ensure that the $j_{\rm eff} = 1/2$ description is appropriate. Although the DP structure does not feature direct edge-sharing IrO_6 octahedra, Kitaev couplings can still arise from multiple extended Ir-O-O-Ir superexchange paths. Indeed, the fcc lattice has been theoretically proposed as a potential venue for realizing Kitaev interactions [25]. The DP fcc structure has new features beyond previous, experimentally studied, candidate Kitaev materials — it contains twelve-fold coordinated Ir sites, has strong geometric frustration, and a larger Ir-Ir distance that should weaken direct exchange.

The significance of the Kitaev interactions in La_2MgIrO_6 and La_2ZnIrO_6 is not at all evident from the observed magnetic ordering. Indeed, as explained in detail below, both materials exhibit A-type (Type-I) antiferromagnetic (AFM) ordering, with transition temperatures $T_N = 12$ and 7.5 K [23, 24, 26]. Such commonly observed magnetic order on the fcc lattice is traditionally ascribed to first and second neighbor Heisenberg exchange interactions [27, 28]. However, as shown in recent work, just the simplest nearest-neighbor AFM Kitaev coupling on the fcc lattice can also stabilize robust A-type AFM [29], which leads us to question this conventional Heisenberg model interpretation of A-type AFM order, especially in $5d$ oxides with strong SOC. The smoking gun signature of the underlying dominant and anisotropic Kitaev interaction is then encoded in the quantum spin fluctuations, and it reveals itself in the magnon spectrum.

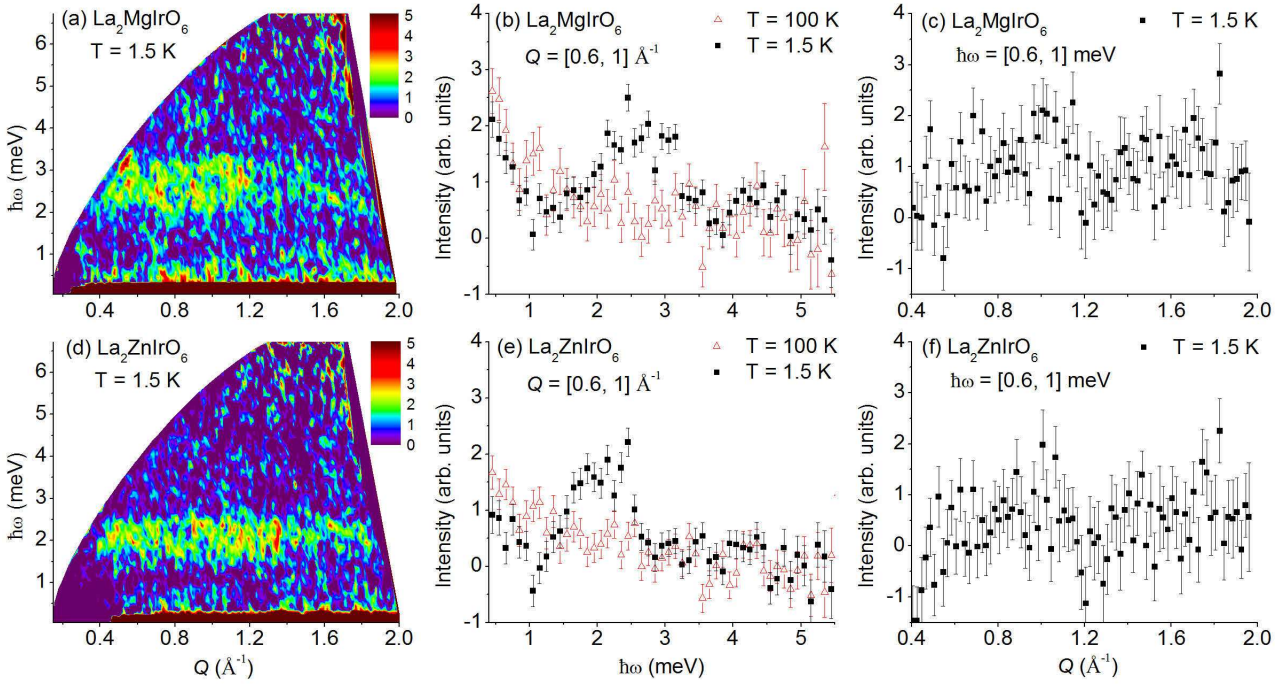

FIG. 1: (a) Color contour plot of HYSPEC data for La_2MgIrO_6 with $E_i = 7.5$ meV and $T = 1.5$ K. An inelastic mode centered at 2.75 meV with weak dispersion is clearly observed. (b) Constant-Q cuts of the HYSPEC data with an integration range of [0.6, 1] Å^{-1} for $T = 1.5$ and 100 K. The low-temperature signal is absent above $T_N = 12$ K, indicating that the mode is magnetic. (c) Constant-$\hbar\omega$ cut of the HYSPEC data with an integration rage of [0.6, 1] meV for $T = 1.5$ K. No inelastic signal is observed near the $Q = 0.79$ Å^{-1} magnetic Bragg peak, indicating that this mode is gapped. (d)-(f) Similar plots for La_2ZnIrO_6 ($T_N = 7.5$ K). A gapped magnetic mode with weak dispersion is also observed in this case, but centered at 2 meV.

In this Letter, we present results from an inelastic neutron scattering (INS) study of the magnetic excitations in La_2BIrO_6. Typically, INS is the most powerful technique to probe magnetic excitations in crystals. However, INS generally has severe limitations in most iridates due to an unfavorable magnetic form factor and the strong neutron absorption cross-section of the Ir nuclei, rendering resonant inelastic x-ray scattering (RIXS) the tool of choice to study magnons [30–32]. Remarkably, we find that La_2BIrO_6 exhibit a clearly observable INS signal, revealing *gapped, highly non-dispersive*, magnons. Our INS work is important since RIXS does not possess the meV resolution to study low energy magnons in a strong Mott insulator. A comparison of our results with a theory of the fcc Kitaev model shows that, counterintuitively, in these materials, even the *conventional* A-type AFM order is driven by *unconventional* interactions.

Magnetic Ordering.— La_2BIrO_6 crystallize in the space group $P2_1/n$ with pseudo-tetragonal lattices due to weak monoclinic structural distortions, and therefore the unit cells can be approximately indexed in tetragonal notation (see Supplemental Material [33] for relationship to fcc unit cell). For La_2MgIrO_6, magnetization measurements show no evidence for a net ferromagnetic (FM) moment, while neutron powder diffraction work finds a magnetic Bragg peak at $Q = 0.79$ Å^{-1} [23] corresponding to A-type AFM order. These combined results are consistent with a magnetic propagation vector of $\vec{k} = (0.5\ 0.5\ 0)_t$ or $(0.5\ \text{-}0.5\ 0)_t$, indicative of FM planes stacked along the $[110]_t$ or $[1\text{-}10]_t$ direction. Although the data do not determine the moment direction unambiguously, electronic structure calculations [23] predict that the moments lie predominantly in the FM planes (A-II type AFM [29]).

For La_2ZnIrO_6, magnetization measurements find evidence for a net FM moment, while neutron diffraction again detects a magnetic Bragg peak at $Q = 0.79$ Å^{-1} [23]. These findings are consistent with a canted A-type AFM characterized by a $\vec{k} = 0$ propagation vector, which defines the c-axis as the FM plane stacking direction. The magnetic Bragg peak is then uniquely indexed as $(001)_t$. The observation of this peak, combined with the absence of the $(100)_t$ and $(010)_t$ peaks, strongly implies that the ordered moments lie in the FM planes. Thus, the A-type AFM in this system also corresponds to A-II. The spin canting in La_2ZnIrO_6 arises from small, staggered IrO_6 octahedral rotations ($\sim 11^\circ$); we ignore this weak canting in our spin wave theory below.

Inelastic Neutron Scattering Data.— We now focus on the magnetic excitations associated with the ordered phases of these materials. Inelastic neutron scattering data were collected on powder samples of La_2BIrO_6 [23], using the HYSPEC spectrometer at Oak Ridge National Laboratory (see Supplemental Material [33] for technical experimental details). A nearly-dispersionless band can be clearly observed in the $T = 1.5$ K inelastic spectrum for each system, as shown

in Fig. 1(a) and (d). Note that the lowest-Q regions in these plots show no intensity; this issue results from a background oversubtraction of the direct beam, which is a consequence of the strong neutron absorption of Ir in the samples. Fig. 1(b) and (e) depict constant Q-cuts at $T = 1.5$ and 100 K with integration ranges of [0.6, 1] Å^{-1}, which place the magnetic Bragg peaks at $Q = 0.79$ Å^{-1} near the center of this region. The excitations are only visible at 1.5 K, confirming their magnetic nature. Furthermore, detailed temperature-dependent measurements on the thermal triple axis spectrometer HB-3 show that these inelastic signals disappear around T_N in each case (see Supplemental Material [33]). The observed temperature dependence of the modes, coupled with the absence of low-lying crystal field levels in a $j_{\text{eff}} = 1/2$ picture, ensure that these nearly-dispersionless excitations correspond to spin waves. Fig. 1(c) and (f) show constant-$\hbar\omega$ cuts at $T = 1.5$ K for the two systems, with an integration range [0.6, 1] meV. We find no evidence for enhanced intensity near the $Q = 0.79$ Å^{-1} magnetic Bragg peaks, which suggests that these excitations are fully gapped. For La_2MgIrO_6 (La_2ZnIrO_6), the low-T constant-Q cuts shown in Fig. 1 reveal that the central position of the mode is 2.75 meV (2 meV), with a bandwidth of 1.5 meV (1 meV). For $j_{\text{eff}} = 1/2$ systems, there is no single ion anisotropy [7]; we therefore explore the origin of the observed spin gaps in more detail below.

Model, Quantum Order by Disorder.— We have previously studied the classical phase diagram for $j_{\text{eff}} = 1/2$ fcc magnets [29], keeping all symmetry-allowed nearest neighbor (NN) interactions. A key finding, relevant to La_2BIrO_6, was that while the simple NN AFM Heisenberg model exhibits A-type AFM order, the exact same order is also favored by just the AFM Kitaev exchange. One might distinguish between these two microscopic mechanisms for the observed order using the frustration parameter, $f \equiv \Theta_{CW}/T_N$, the ratio of the Curie-Weiss temperature Θ_{CW} to the AFM ordering temperature T_N. For the NN Heisenberg model on the fcc lattice, we estimated $f \approx 9$ for spin-1/2 moments [29]. However, La_2BIrO_6 exhibit robust AFM order, with La_2MgIrO_6 having $f \approx 2$, suggesting that SOC-induced Kitaev interactions are large, suppressing frustration and enhancing T_N. This led us to propose a minimal Kitaev model on the ideal fcc lattice,

$$H_K = J_K \sum_{\langle \mathbf{r}\mathbf{r}' \rangle_{xy}} S^z_{\mathbf{r}} S^z_{\mathbf{r}'} + J_K \sum_{\langle \mathbf{r}\mathbf{r}' \rangle_{yz}} S^x_{\mathbf{r}} S^x_{\mathbf{r}'} + J_K \sum_{\langle \mathbf{r}\mathbf{r}' \rangle_{xz}} S^y_{\mathbf{r}} S^y_{\mathbf{r}'} \quad (1)$$

as a better starting point to describe magnetism in La_2BIrO_6. Here, $\langle \mathbf{r}\mathbf{r}' \rangle_{xy}$ denotes nearest neighbors in the xy-plane (similarly for yz, xz). This model has $\Theta_{CW} = -J_K$, so $J_K > 0$ is consistent with the reported $\Theta_{CW} = -24$ K for La_2MgIrO_6 and $\Theta_{CW} = -3$ K for La_2ZnIrO_6 [23]. A classical Monte Carlo study showed that $f \approx 2$ for the AFM Kitaev model, in good agreement with the data on La_2MgIrO_6.

The AFM Kitaev model with $J_K > 0$ on the fcc lattice leads to A-type AFM, with spins in the FM plane (A-II AFM), and therefore it is consistent with the magnetic structures of La_2BIrO_6 described above. However, the classical Kitaev model does not select any special direction in the plane, leading to an accidental XY degeneracy. We study the effect of quantum fluctuations around the ordered A-II AFM state at $T = 0$, using Holstein-Primakoff (HP) bosons. Considering ferromagnetic xy-planes stacked antiferromagnetically along $\hat{z}$, and spins making an angle ϕ with the $\hat{x}$-axis (Ir-O bond direction), linear spin-wave theory (details in Supplemental Material [33]) leads to a magnon dispersion

$$\omega_\phi(\mathbf{k}) = 2J_K \left[(1 + C^{xy}_{\mathbf{k}})(1 + C^{xz}_{\mathbf{k}} \cos^2\phi + C^{yz}_{\mathbf{k}} \sin^2\phi) \right]^{1/2} \quad (2)$$

with $C^{ij}_{\mathbf{k}} = \cos k_i \cos k_j$ ($i = x, y, z$). The zero-point energy of quantum fluctuations, $E_{\text{zp}}(\phi) = \frac{1}{2} \int_{\mathbf{k}} \omega_\phi(\mathbf{k})$ per spin, shows discrete minima at $\phi = n\pi/2$ ($n = 0, 1, 2, 3$). Thus, quantum order by disorder breaks the classical XY degeneracy, leading to spins in the FM plane pointing along the Ir-O bonds.

Gapped Magnons.— The magnon dispersion $\omega_\phi(\mathbf{k})$ obtained in linear spin-wave theory is gapless due to the accidental XY degeneracy of the classical Hamiltonian. Since quantum fluctuations lift this degeneracy, we expect the concomitant development of a magnon gap. To see this in a transparent manner, we expand $E_{\text{zp}}(\phi) \approx E_{\text{zp}}(\phi = 0) + \frac{1}{2}\gamma\phi^2$, where

$$\gamma = J_K \int_{\mathbf{k}} \sqrt{\frac{1 + C^{xy}_{\mathbf{k}}}{1 + C^{xz}_{\mathbf{k}}}} (C^{yz}_{\mathbf{k}} - C^{xz}_{\mathbf{k}}). \quad (3)$$

This leads to a pinning field $2\gamma \approx 0.2 J_K$ in the ordered state, opening up a magnon gap. Such an order-by-disorder gap was discussed within a different model for $LaTiO_3$ [34]; however, SOC in $LaTiO_3$ is weak, leading to a tiny gap for highly dispersive magnons. Here, by contrast, the magnon gap and dispersion are both determined by the *same* interaction, J_K.

The magnon gap appears naturally upon incorporating spin-wave interactions. We study this using a self-consistent mean field Hamiltonian approach (see Supplemental Material [33])

$$H_{\text{mft}} = \sum_{\mathbf{k}>0} \begin{pmatrix} a^\dagger_{\mathbf{k}} & a_{-\mathbf{k}} \end{pmatrix} \begin{pmatrix} A_{\mathbf{k}} & B_{\mathbf{k}} \\ B_{\mathbf{k}} & A_{\mathbf{k}} \end{pmatrix} \begin{pmatrix} a_{\mathbf{k}} \\ a^\dagger_{-\mathbf{k}} \end{pmatrix} \quad (4)$$

with $A_{\mathbf{k}} = (2 + C_{xy} + C_{xz}) + \delta A_{\mathbf{k}}$, $B_{\mathbf{k}} = (C_{xz} - C_{xy}) + \delta B_{\mathbf{k}}$, and

$$\begin{aligned} \delta A_{\mathbf{k}} &= 2(\bar{F}_{xy} - \bar{F}_{xz}) + \bar{F}(C_{xy} - C_{xz}) - 2\bar{G}(C_{xy} + C_{xz}) \\ &- 2(\bar{G}_{xy} + \bar{G}_{xz}) - 4\bar{G} - 4\bar{G}_{yz} C_{yz} \quad (5) \\ \delta B_{\mathbf{k}} &= (\bar{G}_{xy} - \bar{G}_{xz}) + 2\bar{G}(C_{xy} - C_{xz}) - \bar{F}(C_{xy} + C_{xz}) \\ &- (\bar{F}_{xy} + \bar{F}_{xz}) - 4\bar{F}_{yz} C_{yz}. \quad (6) \end{aligned}$$

Here, $\bar{F} \equiv \int_{\mathbf{k}} F_{\mathbf{k}}$, $\bar{F}_{ij} \equiv \int_{\mathbf{k}} C^{ij}_{\mathbf{k}} F_{\mathbf{k}}$, and similarly for G, with $F_{\mathbf{k}} = \sinh 2\varphi_{\mathbf{k}}$, $G_{\mathbf{k}} = (\cosh 2\varphi_{\mathbf{k}} - 1)/2$, the renormalized dispersion $\Omega_{\mathbf{k}} = \sqrt{A^2_{\mathbf{k}} - B^2_{\mathbf{k}}}$, $\cosh 2\varphi_{\mathbf{k}} = A_{\mathbf{k}}/\Omega_{\mathbf{k}}$, and $\sinh 2\varphi_{\mathbf{k}} = -B_{\mathbf{k}}/\Omega_{\mathbf{k}}$. Using these equations, we determine $F_{\mathbf{k}}, G_{\mathbf{k}}$ self-consistently. The resulting powder averaged dynamic structure factor $S(Q, \omega)$, convolved with the Gaussian instrumental energy resolution, is plotted in Fig. 2(b), showing clear evidence of a gapped magnon band.

In Fig. 2(a), we compare this result to a J_1-J_2 Heisenberg model with nearest AFM exchange $J_1 > 0$, and next-neighbor

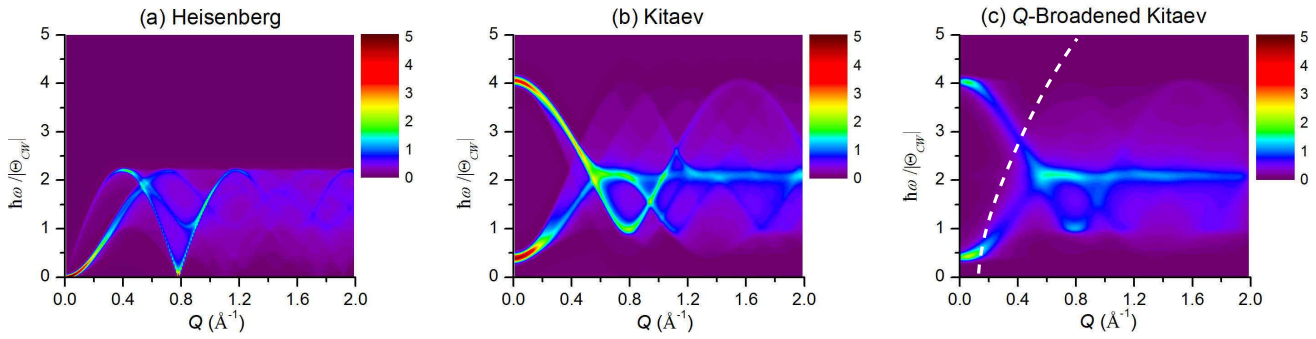

FIG. 2: Color contour plots of the theoretically calculated powder-averaged $S(Q,\omega)$ for (a) the J_1-J_2 Heisenberg model with $J_1 > 0$ and $J_2 = -J_1/2$, (b) the Kitaev model with $J_K > 0$, and (c) the Kitaev model including momentum-broadening. The energy scale is normalized by the appropriate Curie-Weiss temperature, with $\Theta_{CW} = -3J_1 - 3J_2/2$ for the Heisenberg model and $\Theta_{CW} = -J_K$ for the Kitaev model. The Kitaev model reproduces the weakly dispersive spin gapped mode observed in the INS data. The dashed white curve in (c) represents the low angle detector limit of the HYSPEC INS data shown in Fig.1; note that the energy scale of this curve is in absolute units of meV.

FM exchange $J_2 < 0$, which has $\Theta_{CW} = -3J_1 - 3J_2/2$. We fix $J_2 = -0.5J_1$, which appears unphysically large [35], but chosen since it leads to a small frustration parameter $f \approx 2$, just as for the pure AFM Kitaev model. In this Heisenberg case, $S(Q,\omega)$ exhibits a clear signature of the gapless Goldstone mode despite the powder averaging. Such low energy excitations are ruled out by our INS data. Furthermore, this model shows no clear, flat band of intensity centered about a particular energy transfer, in contrast to INS observations.

Discussion.— The qualitative agreement between our INS data and theoretical results above on gapped magnons lends strong support to the Kitaev model as the correct microscopic theory. Incorporating weak Heisenberg or off-diagonal symmetric exchange (ODSE) [12, 29] does not significantly change our results. Large ODSE leads to distinct AFM order [29] which is ruled out by neutron diffraction [23]. However, the excitation spectrum of the Kitaev model in Fig. 2(b) shows sharp dispersive features which are absent in the data. We ascribe this difference to weak B/B′ anti-site disorder, a common defect in DPs [36, 37], which may wash out sharp features; a structural refinement of x-ray diffraction data on our samples (see Supplemental Material [33]) yields an average defect density $n_{\rm d} \sim 6\%$. This should lead to magnon scattering, with a mean free path $\ell \sim n_d^{-1/3} a_0$, where the Ir-Mg bond length $a_0 \approx 3.95$ Å. We treat disorder in a heuristic manner, assuming it leads to a Lorentzian momentum broadening of the calculated spectrum, with a full-width half-maximum (FWHM) $\Delta Q = 1/\ell$. From Fig. 2(c), the resulting $S(Q,\omega)$, with $\Delta Q = 0.1$ Å^{-1}, shows better agreement with the INS data. However, minor differences remain, calling for a careful treatment of disorder as well as magnon interaction effects.

Our theory focuses on the perfect fcc crystal, so that anisotropies between exchange couplings in different directions are ignored and antisymmetric Dzyaloshinskii-Moriya (DM) interactions are forbidden by inversion symmetry. In reality, octahedral rotations reduce the crystal symmetry in La_2BIrO_6 to monoclinic *P2$_1$/n*; a more complete theory [38] must account for this. However, (i) the octahedral rotations in La_2ZnIrO_6 and La_2MgIrO_6 are small (see Supplemental Material [33] and Refs. [23, 29]), and (ii) their INS data above look remarkably similar despite a larger distortion in La_2ZnIrO_6. We thus expect these distortions to only lead to small corrections to the ideal cubic limit. Previous work on Sr_2IrO_4 shows that strong SOC leads to moments which track the IrO_6 octahedral rotations, such that the DM interactions due to distortions arise from local unitary rotations on the $j_{\rm eff} = 1/2$ Heisenberg model [7]. This 'hidden' Heisenberg symmetry [7, 39] explains the existence of highly dispersive and nearly-gapless magnetic excitations in Sr_2IrO_4 [30, 40, 41]. Thus, the observed spin gaps in La_2BIrO_6 cannot simply be attributed to DM interactions induced by *P2$_1$/n* distortions. We have also checked that the fcc Heisenberg model with weak anisotropic couplings induced by small *P2$_1$/n* distortions [38, 42] cannot simultaneously explain the observed gapped $S(Q,\omega)$ mode and thermodynamics (Θ_{CW} and T_N).

Having argued that Kitaev interactions dominate in La_2BIrO_6, we estimate J_K by comparing our Kitaev model results to the INS data. Scaling the results in Fig. 2(c) so that the most intense region of the computed magnon band at $\hbar\omega/|\Theta_{CW}| \approx 2$ matches up with the center (top) of the band observed with INS, we find that $J_K \approx 1.4$ and 1 meV (1.8 and 1.3 meV) respectively for La_2MgIrO_6 and La_2ZnIrO_6. These values are in reasonable agreement with our earlier estimates [29] from thermodynamics [43]. The smaller J_K for La_2ZnIrO_6 is consistent with its lower T_N. Our key finding is that the Kitaev interactions are AFM and dominant in both materials; similar conclusions based on INS data were reported recently for the 2D honeycomb material α-$RuCl_3$ [16].

Conclusions.— Our combined INS data and spin wave calculations show that La_2BIrO_6 are rare examples of materials with strong Kitaev exchange. This unconventional exchange on the fcc lattice leads to AFM order, rather than an exotic quantum spin liquid. The dominance of the Kitaev term may be due to extended Ir-O-O-Ir superexchange pathways, suggesting that this presents a promising framework to look for exotic Kitaev materials on different lattice geometries.

We thank M.D. Lumsden for useful discussions and V. O. Garlea for technical support. This research was supported by the US Department of Energy (DOE), Office of Basic Energy Sciences. A.A.A., S.C. and A.D.C were supported by the Scientific User Facilities Division. G.-X.C. and D.M. were supported by the Materials Science and Engineering Division. T.J.W. acknowledges support from the Wigner Fellowship program at ORNL. The neutron experiments were performed at the Spallation Neutron Source and the High Flux Isotope Reactor, which are sponsored by the Scientific User Facilities Division. A.M.C. Y.B.K., and A.P. were funded by NSERC of Canada.

* author to whom correspondences should be addressed: E-mail:[aczelaa@ornl.gov]

† author to whom correspondences should be addressed: E-mail:[arunp@physics.utoronto.ca]

[1] B.J. Kim *et al*, Phys. Rev. Lett. **101**, 076402 (2008).
[2] F. Wang and T. Senthil, Phys. Rev. Lett. **106**, 136402 (2011).
[3] B.-J. Yang and Y.B. Kim, Phys. Rev. B **82**, 085111 (2010).
[4] D. Pesin and L. Balents, Nature Physics **6**, 376 (2010).
[5] J.-M. Carter, V.V. Shankar, M.A. Zeb, and H.-Y. Kee, Phys. Rev. B **85**, 115105 (2012).
[6] X. Wan, A.M. Turner, A. Vishwanath, and S.Y. Savrasov, Phys. Rev. B **83**, 205101 (2011).
[7] G. Jackeli and G. Khaliullin, Phys. Rev. Lett. **102**, 017205 (2009).
[8] A. Kitaev, Annals of Physics **321**, 2 (2006).
[9] Y. Singh, S. Manni, J. Reuther, T. Berlijn, R. Thomale, W. Ku, S. Trebst, and P. Gegenwart, Phys. Rev. Lett. **108**, 127203 (2012).
[10] Y. Singh and P. Gegenwart, Phys. Rev. B **82**, 064412 (2010).
[11] K.W. Plumb, J.P. Clancy, L.J. Sandilands, V.V. Shankar, Y.F. Hu, K.S. Burch, H.-Y. Kee, and Y.-J. Kim, Phys. Rev. B **90**, 041112(R) (2014).
[12] J. G. Rau, E.K.-H. Lee, and H.-Y. Kee, Phys. Rev. Lett. **112**, 077204 (2014).
[13] F. Ye, S. Chi, H. Cao, B.C. Chakoumakos, J.A. Fernandez-Baca, R. Custelcean, T.F. Qi, O.B. Korneta, and G. Cao, Phys. Rev. B **85**, 180403(R) (2012).
[14] J.A. Sears, M. Songvilay, K.W. Plumb, J.P. Clancy, Y. Qiu, Y. Zhao, D. Parshall, and Y.-J. Kim, Phys. Rev. B **91**, 144420 (2015).
[15] L.J. Sandilands, Y. Tian, K.W. Plumb, Y.-J. Kim, and K.S. Burch, Phys. Rev. Lett. **114**, 147201 (2015).
[16] A. Banerjee, C.A. Bridges, J.-Q. Yan, A.A. Aczel, L. Li, M.B. Stone, G.E. Granroth, M.D. Lumsden, Y. Yiu, J. Knolle, D.L. Kovrizhin, S. Bhattacharjee, R. Moessner, D.A. Tennant, D.G. Mandrus, and S.E. Nagler, arXiv: 1504.08037 (unpublished).
[17] T. Takayama, A. Kato, R. Dinnebier, J. Nuss, H. Kono, L.S.I. Veiga, G. Fabbris, D. Haskel, and H. Takagi, Phys. Rev. Lett. **114**, 077202 (2015).
[18] K.A. Modic *et al*, Nature Communications **5**, 4203 (2014).
[19] A. Biffin, R.D. Johnson, S. Choi, F. Freund, S. Manni, A. Bombardi, P. Manuel, P. Gegenwart, and R. Coldea, Phys. Rev. B **90**, 205116 (2014).
[20] A. Biffin, R.D. Johnson, I. Kimchi, R. Morris, A. Bombardi, J.G. Analytis, A. Vishwanath, and R. Coldea, Phys. Rev. Lett. **113**, 197201 (2014).
[21] A.V. Powell, J.G. Gore, and P.D. Battle, Journal of Alloys and Compounds **201**, 73 (1993).
[22] R.C. Currie, J.F. Vente, E. Frikkee, and D.J.W. Ijdo, Journal of Solid State Chemistry **116**, 199 (1995).
[23] G. Cao, A. Subedi, S. Calder, J.-Q. Yan, J. Yi, Z. Gai, L. Poudel, D.J. Singh, M.D. Lumsden, A.D. Christianson, B.C. Sales, and D. Mandrus, Phys. Rev. B **87**, 155136 (2013).
[24] W.K. Zhu, C.-K. Lu, W. Tong, J.M. Wang, H.D. Zhou, and S.X. Zhang, Phys. Rev. B **91**, 144408 (2015).
[25] I. Kimchi and A. Vishwanath, Phys. Rev. B **89**, 014414 (2014).
[26] Ref. [24] suggests that there are actually two different magnetic transition temperatures in close proximity for La_2ZnIrO_6 ($T_1 = 7.3$ K and $T_2 = 8.5$ K), but this finding is not important for the results presented in our work.
[27] M.S. Seehra and T.M. Giebultowicz, Phys. Rev. B **38**, 11898 (1988).
[28] K. Lefmann and C. Rischel, Eur. Phys. J. B **21**, 313 (2001).
[29] A.M. Cook, S. Matern, C. Hickey, A.A. Aczel, and A. Paramekanti, arXiv:1502.01031 (unpublished).
[30] J. Kim *et al*, Phys. Rev. Lett. **108**, 177003 (2012).
[31] J. Kim *et al*, Phys. Rev. Lett. **109**, 157402 (2012).
[32] H. Gretarsson *et al*, Phys. Rev. B **87**, 220407(R) (2013).
[33] See Supplemental Material at http://link.aps.org/supplemental/xx.xxxx/PhysRevLett.xx.xxxxxx for additional details about (i) crystal structure information of La_2BIrO_6, (ii) technical aspects of the INS experiments, (iii) results from the HB-3 neutron scattering measurement, and (iv) calculations of quantum order by disorder and magnon interaction effects.
[34] G. Khaliullin, Phys. Rev. B **64**, 212405 (2001).
[35] S. Baidya and T. Saha-Dasgupta, Phys. Rev. B **86**, 024440 (2012).
[36] Q.S. Lin, M. Greenblatt, E.N. Caspi, and M. Avdeev, Journal of Solid State Chemistry **179**, 2086 (2006).
[37] T. Aharen, J.E. Greedan, C.A. Bridges, A.A. Aczel, J. Rodriguez, G. MacDougall, G.M. Luke, T. Imai, V.K. Michaelis, S. Kroeker, H.D. Zhou, C.R. Wibe, and L.M.D. Cranswick, Phys. Rev. B **81**, 224409 (2010).
[38] H. Ishizuka and L. Balents, Phys. Rev. B **90**, 184422 (2014).
[39] F. Wang and T. Senthil, Phys. Rev. Lett. **106**, 136402 (2011).
[40] S. Fujiyama, H. Oshumi, T. Komesu, J. Matsuno, B.J. Kim, M. Takata, T. Arima, and H. Takagi, Phys. Rev. Lett. **108**, 247212 (2012).
[41] S. Bahr, A. Alfonsov, G. Jackeli, G. Khaliullin, A. Matsumoto, T. Takayama, H. Takagi, B. Buchner, and V. Kataev, Phys. Rev. B **89**, 180401(R) (2014).
[42] E.V. Kuz'min, S.G. Ovchinnikov, and D.J. Singh, Phys. Rev. B **68**, 024409 (2003).
[43] Our preliminary estimates of J_K in Ref. [29] relied on the Curie-Weiss temperatures Θ_{CW} reported in Ref. [23]. However, Θ_{CW} from a magnetic susceptibility measurement can vary by a few K, depending on the temperature fitting range, the sample mount used, and the applied field. INS provides a more accurate measurement of the exchange constants for a magnetic system.

A. Crystal Structure Information

La_2MgIrO_6 and La_2ZnIrO_6 crystallize in the monoclinic space group $P2_1/n$ arising from small structural distortions to the ideal face-centered cubic (fcc) double perovskite structure. The unit cell associated with the $P2_1/n$ space group is a superstructure of the primitive cubic unit cell, and the superstructure can be approximately indexed in tetragonal notation due

to the small monoclinic distortions. Assuming that $\hat{x}$, $\hat{y}$, and $\hat{z}$ are aligned with the three fcc crystallographic directions, the relationships between the tetragonal and fcc lattice constants are as follows: $\vec{a}_t = \frac{a_{fcc}}{2}(\hat{x} \pm \hat{y})$ and $\vec{c}_t = a_{fcc}\hat{z}$. Note that $a_{fcc} \approx 7.9$ Å for these systems [1].

B/B′ site mixing is often an important consideration to take into account when performing structural refinements of double perovskite data, but this possibility was neglected recently in structural refinements of these materials presented in Ref. [1]. For this reason, we have revisited the x-ray diffraction data presented in that paper and performed new structural refinements, with the site mixing now included as a fitting parameter. We find a B/B′ site mixing value of 8% and 5% for the Mg and Zn systems respectively, with lattice constants and atomic fractional coordinates essentially identical to the values reported in Ref. [1].

We now make an effort here to quantify the effects of the monoclinic structural distortions on the IrO_6 octahedra. There are two main effects: the rotation of the octahedra about both the cubic [110] and c-axes, and the deformation of the Ir^{4+} local environment away from ideal cubic due to elongation/compression of the octahedra along different directions. The rotation angles of the IrO_6 octahedra can be determined according to Ref. [2] by using the refined atomic fractional coordinates and the Glazer notation discussed in Refs. [3, 4]. We find that the IrO_6 octahedra have global rotations of 13° and 14° for the Mg and Zn systems respectively about the cubic [110] axis, and rotations of 9° and 11° respectively about the c-axis that are staggered between adjacent ab-layers. The deformation of the IrO_6 octahedra can be quantified by considering the three different Ir-O bonds. From the structural refinements, we find that all three types of Ir-O bond lengths are within 1% of each other for both systems. This implies a nearly ideal cubic local environment for the Ir^{4+} ions.

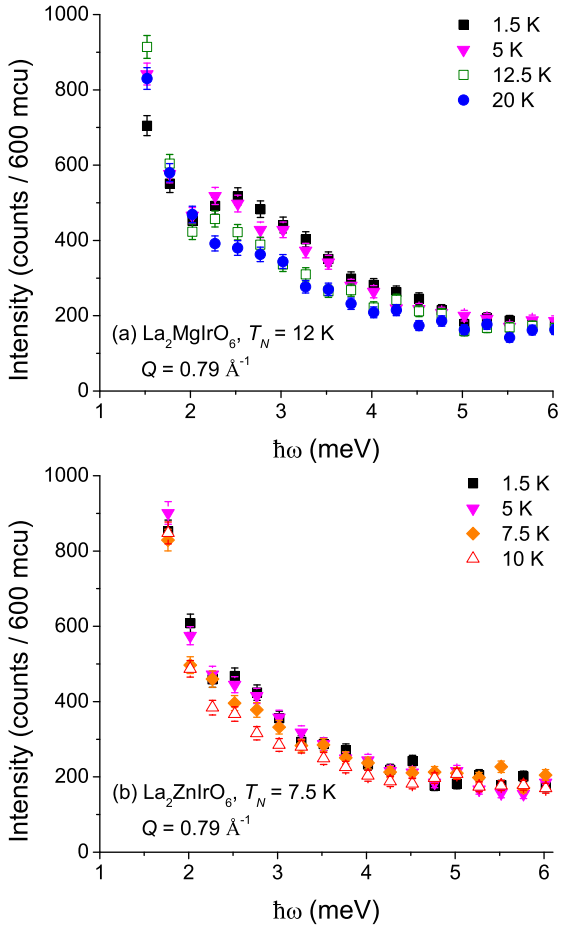

FIG. 3: HB-3 constant-Q scans with $Q = 0.79$ Å^{-1} for (a) La_2MgIrO_6 and (b) La_2ZnIrO_6 at selected temperatures. The magnetic signals disappear around T_N for each compound, indicating that the modes have a spin wave origin. Note that 1 mcu ≈ 10000 and 11000 monitor counts for the Mg and Zn data respectively.

B. Technical Details of Neutron Scattering Experiments

Inelastic neutron scattering data were collected on powder samples of La_2MgIrO_6 and La_2ZnIrO_6 at the HYSPEC spectrometer of the Spallation Neutron Source, Oak Ridge National Lab (ORNL). The powder samples were loaded in Al annular cans to minimize neutron absorption. All data were collected using an incident energy $E_i = 7.5$ meV with the Fermi chopper spinning at 240 Hz, resulting in an instrumental energy resolution of 0.25 meV (Gaussian full-width half-maximum [FWHM]) at the elastic line. The Q-resolution at the elastic line was found to be 0.03 Å^{-1} (Gaussian FWHM) by fitting nuclear Bragg peaks from the samples to Gaussian functions. A He cryostat was used to achieve a base temperature of 1.5 K. Empty Al annular can measurements were subtracted from all the HYSPEC data presented in this work, so the Al scattering contribution to the sample spectra would be minimized.

Detailed temperature-dependent measurements of the La_2MgIrO_6 and La_2ZnIrO_6 magnetic excitations were also collected in a He cryostat on the thermal triple axis spectrometer HB-3 at the High Flux Isotope Reactor of ORNL. A collimation of 48'-60'-60'-120' and a fixed final energy of $E_f = 14.7$ meV were used to achieve an energy resolution of 1.2 meV at the elastic line (Gaussian FWHM).

C. HB-3 Triple Axis Neutron Scattering Data

Fig. 3 presents constant-Q scans at a magnetic zone center ($Q = 0.79$ Å^{-1}) for (a) La_2MgIrO_6 and (b) La_2ZnIrO_6. The two panels provide strong evidence that the observed modes correspond to spin wave excitations associated with the ordered states for these systems, as the magnetic signal disappears around T_N in each case.

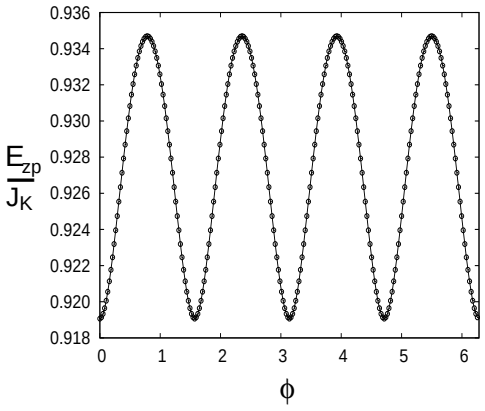

FIG. 4: Plot of the ϕ-dependent zero point energy contribution $E_{\rm zp}$ (in units of J_K) for the Kitaev model, showing minima at discrete values of $\phi = n\pi/2$ ($n = 0, 1, 2, 3$) which leads to quantum order by disorder with spins pointing along the Ir-O bond directions.

D. Quantum Order By Disorder

Assuming that the spins in the AFM A-II state lie in the cubic xy plane, and make an angle ϕ with the x-axis, the classical ground state energy is independent of ϕ. We evaluate the contribution from zero point fluctuations using a standard Holstein-Primakoff linear spin wave expansion, setting

$$S^x_{\mathbf{r}} = (-1)^z(\frac{1}{2} - a^\dagger_{\mathbf{r}}a_{\mathbf{r}})\cos\phi - \frac{1}{2}(a_{\mathbf{r}} + a^\dagger_{\mathbf{r}})\sin\phi \quad (7)$$

$$S^y_{\mathbf{r}} = \frac{1}{2}(a_{\mathbf{r}} + a^\dagger_{\mathbf{r}})\cos\phi + (-1)^z(\frac{1}{2} - a^\dagger_{\mathbf{r}}a_{\mathbf{r}})\sin\phi \quad (8)$$

$$S^z_{\mathbf{r}} = (-1)^z\frac{1}{2i}(a_{\mathbf{r}} - a^\dagger_{\mathbf{r}}) \quad (9)$$

This leads to a spin wave energy

$$\omega_\phi(\mathbf{k}) = 2J_K\left[(1+C^{xy}_{\mathbf{k}})(1+C^{xz}_{\mathbf{k}}\cos^2\phi + C^{yz}_{\mathbf{k}}\sin^2\phi)\right]^{1/2} \quad (10)$$

with $C^{ij}_{\mathbf{k}} = \cos k_i \cos k_j$ ($i = x, y, z$). The zero-point energy of quantum fluctuations is $E_{\rm zp}(\phi) = \frac{1}{2}\int_{\mathbf{k}}\omega_\phi(\mathbf{k})$ per spin. We plot $E_{\rm zp}(\phi)$ in Fig. 4, showing that it has discrete minima at $\phi = n\pi/2$ ($n = 0, 1, 2, 3$). Quantum fluctuations in the presence of SOC thus break the accidental classical degeneracy in ϕ, favoring spins to point along the Ir-O bond directions in the FM plane.

E. Mean field theory of gapped magnons

Beyond linear spin waves, we set

$$S^x_{\mathbf{r}} = (-1)^z(\frac{1}{2} - a^\dagger_{\mathbf{r}}a_{\mathbf{r}}) \quad (11)$$

$$S^y_{\mathbf{r}} = \frac{1}{2}(a_{\mathbf{r}} + a^\dagger_{\mathbf{r}}) - \frac{1}{4}(a^\dagger_{\mathbf{r}}a_{\mathbf{r}}a_{\mathbf{r}} + a^\dagger_{\mathbf{r}}a^\dagger_{\mathbf{r}}a_{\mathbf{r}}) \quad (12)$$

$$S^z_{\mathbf{r}} = (-1)^z\left[\frac{1}{2i}(a_{\mathbf{r}} - a^\dagger_{\mathbf{r}}) - \frac{1}{4i}(a^\dagger_{\mathbf{r}}a_{\mathbf{r}}a_{\mathbf{r}} - a^\dagger_{\mathbf{r}}a^\dagger_{\mathbf{r}}a_{\mathbf{r}})\right] \quad (13)$$

and expand the Hamiltonian, only keeping terms to quartic order, which we decouple using mean field parameters $F_{\mathbf{k}} = \langle a^\dagger_{\mathbf{k}}a^\dagger_{-\mathbf{k}}\rangle$ and $G_{\mathbf{k}} = \langle a^\dagger_{\mathbf{k}}a_{\mathbf{k}}\rangle$. This leads to the Hamiltonian

$$H_{\rm mft} = \sum_{\mathbf{k}>0}\begin{pmatrix} a^\dagger_{\mathbf{k}} & a_{-\mathbf{k}}\end{pmatrix}\begin{pmatrix} A_{\mathbf{k}} & B_{\mathbf{k}} \\ B_{\mathbf{k}} & A_{\mathbf{k}}\end{pmatrix}\begin{pmatrix} a_{\mathbf{k}} \\ a^\dagger_{-\mathbf{k}}\end{pmatrix} \quad (14)$$

with $A_{\mathbf{k}} = (2 + C_{xy} + C_{xz}) + \delta A_{\mathbf{k}}$, $B_{\mathbf{k}} = (C_{xz} - C_{xy}) + \delta B_{\mathbf{k}}$, and

$$\delta A_{\mathbf{k}} = 2(\bar{F}_{xy} - \bar{F}_{xz}) + \bar{F}(C_{xy} - C_{xz}) - 2\bar{G}(C_{xy} + C_{xz}) - 2(\bar{G}_{xy} + \bar{G}_{xz}) - 4\bar{G} - 4\bar{G}_{yz}C_{yz} \quad (15)$$

$$\delta B_{\mathbf{k}} = (\bar{G}_{xy} - \bar{G}_{xz}) + 2\bar{G}(C_{xy} - C_{xz}) - \bar{F}(C_{xy} + C_{xz}) - (\bar{F}_{xy} + \bar{F}_{xz}) - 4\bar{F}_{yz}C_{yz}. \quad (16)$$

Here, we have defined averages $\bar{F} \equiv \int_{\mathbf{k}} F_{\mathbf{k}}$, $\bar{F}_{ij} \equiv \int_{\mathbf{k}} C^{ij}_{\mathbf{k}} F_{\mathbf{k}}$, and similarly for $G_{\mathbf{k}}$. Requiring self-consistency, we set $F_{\mathbf{k}} = \sinh 2\varphi_{\mathbf{k}}$ and $G_{\mathbf{k}} = (\cosh 2\varphi_{\mathbf{k}} - 1)/2$, with the renormalized dispersion $\Omega_{\mathbf{k}} = \sqrt{A^2_{\mathbf{k}} - B^2_{\mathbf{k}}}$, $\cosh 2\varphi_{\mathbf{k}} = A_{\mathbf{k}}/\Omega_{\mathbf{k}}$, and $\sinh 2\varphi_{\mathbf{k}} = -B_{\mathbf{k}}/\Omega_{\mathbf{k}}$. To solve these equations, we begin with a guess for the Hamiltonian matrix of the form $\delta A_{\mathbf{k}} = \gamma$, and $\delta B_{\mathbf{k}} = 0$, where γ represents the effect of the pinning field arising from order by disorder as described in the text, and iterate the mean field equations to achieve self-consistency.

Using the converged result, we compute the renormalized staggered magnetization, and find $m_{\rm AF} \approx 0.46$ in the ideal fcc lattice Kitaev model, leading to $\sim 8\%$ suppression of the classical $j_{\rm eff} = 1/2$ order parameter due to quantum fluctuations. Taking into account the staggered octahedral rotation $\approx 11^\circ$, this $0.92\mu_B$ staggered magnetization translates into a uniform magnetization $\approx 0.18\mu_B$, which roughly agrees with the measured value $\approx 0.22\mu_B$ in La_2ZnIrO_6.

We can use these converged results to also compute the resulting dynamic structure factor, which has components

$$\mathcal{S}_x(\mathbf{k},\omega) = \frac{1}{4}\int\frac{d^3\mathbf{p}}{(2\pi)^3}(\sinh 2\varphi_{\mathbf{p}}\sinh 2\varphi_{\mathbf{k}+\mathbf{p}+\mathbf{Q}} + 4\cosh^2\varphi_{\mathbf{p}}\sinh^2\varphi_{\mathbf{k}+\mathbf{p}+\mathbf{Q}})\delta(\omega - \Omega_{\mathbf{p}} - \Omega_{\mathbf{k}+\mathbf{p}+\mathbf{Q}}) \quad (17)$$

$$\mathcal{S}_y(\mathbf{k},\omega) = (\cosh 2\varphi_{\mathbf{k}} + \sinh 2\varphi_{\mathbf{k}})(1 - 2\bar{G} - \bar{F})\delta(\omega - \Omega_{\mathbf{k}}) \quad (18)$$

$$\mathcal{S}_z(\mathbf{k},\omega) = (\cosh 2\varphi_{\mathbf{k}} - \sinh 2\varphi_{\mathbf{k}})(1 - 2\bar{G} + \bar{F})\delta(\omega - \Omega_{\mathbf{k}+\mathbf{Q}}) \quad (19)$$

where the first term corresponds to longitudinal fluctuations while the latter two correspond to transverse fluctuations. We find, numerically, that the longitudinal fluctuations make a very small contribution to the structure factor, and can be ignored in practice. Powder averaging leads to $S(Q,\omega)$, which is convoluted with a Gaussian function representing the instrumental energy resolution, and plotted in Fig. 2(b) of the main manuscript.

* author to whom correspondences should be addressed: E-mail:[aczelaa@ornl.gov]

† author to whom correspondences should be addressed: E-mail:[arunp@physics.utoronto.ca]

[1] G. Cao, A. Subedi, S. Calder, J.-Q. Yan, J. Yi, Z. Gai, L. Poudel, D.J. Singh, M.D. Lumsden, A.D. Christianson, B.C. Sales, and D. Mandrus, Phys. Rev. B **87**, 155136 (2013).
[2] W.A. Groen, F.P.F. van Berkel, and D.J.W. Ijdo, Acta Cryst. C **42**, 1472 (1986).
[3] A.M. Glazer, Acta Cryst. B **28**, 3384.
[4] P.M. Woodward, Acta. Cryst. B **53**, 32.